Journal of Applied Polymer Science

Morphological and nanomechanical characterization of anisotropic interfacial characteristic regions in CF/PA6 composites at different cooling rates

H. Li,[1] Y. Zhang,[1] G. Bai,[2] B. Zhang[1]
[1]School of Materials Science and Engineering, Beihang University, Beijing 100191, China
[2]Science and Technology on Space Physics Laboratory, Beijing 100076, China
Correspondence to: H. Li (E-mail: li_hongfu@126.com)

ABSTRACT: Macroscopic tensile tests on neat PA6 and CF/PA6 prepregs showed that the cooling rate significantly affects the mechanical properties of CF/PA6 composites because of their different crystallization behaviors both at the fiber surface and in the matrix. Polarizing optical microscopy, static nanoindentation (SNI), and dynamic mechanical imaging (DMI) tests were used to characterize the anisotropic morphologies and nanomechanical performances of the interfacial characteristic regions in CF/PA6 composites at five different cooling rates. As a result, the seven interfacial characteristic regions inside the CF/PA6 composites were clearly distinguished. The interphase thickness of the CF/PA6 composites decreased with a decrease in the cooling rate. On the contrary, the interphase modulus and transcrystallinity thickness and modulus showed significant increases with a decrease in the cooling rate. The DMI and SNI test results were in agreement with each other and with the macromechanical test results. © 2016 Wiley Periodicals, Inc. J. Appl. Polym. Sci. **2016**, *133*, 44106.

KEYWORDS: crystallization; morphology; properties and characterization; surfaces and interfaces; thermoplastics

Received 16 February 2016; accepted 12 June 2016
DOI: 10.1002/app.44106

INTRODUCTION

In recent years, owing to the increasing awareness on environmental protection, the use of recyclable thermoplastics has gained immense attention for manufacturing fiber reinforced composites.[1–3] Polyamide 6 (PA6) is an important engineering plastic with high strength, excellent corrosion resistance, suitable wear resistance, and favorable self-lubricating properties. Hence, carbon fiber reinforced polyamide 6 (CF/PA6) composites have great potential for replacing aluminum in the automotive industry for cost and weight savings.[4]

The stress distribution and properties of composites are significantly influenced by the transit interphase between the matrix and reinforced fiber.[5–7] For example, the thickness and modulus of the interphase should be optimized to achieve improved load transfer efficiency and impact toughness.[8–10] However, inconsistencies still exist in stress transfer and interfacial shear strength (IFSS), which are affected by the interphase thickness and modulus. On the basis of finite element analysis, it has been suggested that a low interphase thickness and high interphase modulus results in efficient stress transfer.[11,12] On the contrary, when the interphase is stiffer than the matrix, an increase in the interphase modulus does not always result in an increase in the stress transfer efficiency, and an optimum modulus ratio of the interphase to the matrix is obtained.[13–16] However, Yu suggested that the interphase thickness and modulus do not influence the shear stress distribution significantly.[17]

Apart from the interphase thickness and modulus, transcrystallinity (TC) thickness and modulus also have a significant effect on the ultimate properties of fiber reinforced thermoplastic composites.[18] For example, a thick transcrystalline layer increases the stress transfer, probably because of the increased radial compressive stresses.[19] On the other hand, an opposite effect is observed when large thermal stresses build up during the transcrystallization process, leading to a reduction in the IFSS.[20] According to the previous reports, a 50-nm-thick transcrystalline layer results in an additional 5% enhancement in the overall composite modulus because the modulus of such crystalline regions is greater than that of the bulk polymer.[21,22] However, there are inconsistencies in the reported absolute values of the modulus ratio because of different composite systems and evaluation methods.[22–27]

In thermoplastic composites, the aforementioned interfacial characteristics are greatly dominated by variations in the thermal processing histories such as cooling rate.[20,28,29] Thus, the

knowledge of interfacial structures and mechanical properties together with the influences of the thermal history on them helps in understanding and tailoring the composite properties better.

In this work, the tensile failure mechanisms of neat PA6 and CF/PA6 prepregs at five different cooling rates was investigated. Their anisotropic interfacial morphology and nanomechanical behaviors were also investigated by using polarizing optical microscopy (POM) and static nanoindentation (SNI), respectively. The dynamic mechanical imaging (DMI) method, which can extract the entire interphase dimension and analyze it quantitatively,[8,30,31] was used to obtain the interphase thickness and modulus of each characteristic region. Finally, the effect of cooling rate on the macromechanical tensile behaviors of neat PA6 and CF/PA6 prepregs was explained by the variation of nanomechanical interfacial properties.

EXPERIMENTAL

Materials

Carbon fiber of Toray T700SC-12K was used as the reinforced fiber. Extrusion grade low viscosity PA 6 granules of UBE 1013B were selected for the matrix.

Cooling Rate Control

Five different nonisothermal cooling rates were chosen in this study. To control the cooling rate of the specimens with different sizes accurately, the cooling history was monitored and controlled using a fast data acquisition system with a μ-thermocouple embedded in a specimen or attached on the surface of the specimen. Five cooling procedures were employed namely, water-quenching (C1), air (C2), thin insulation cotton (C3), thick insulation cotton (C4), and furnace (C5) cooling, and the time required for cooling the specimens to the glass transition temperature (T_g) of about 58 °C using these methods was 15 s, 2.7 min, 21.5 min, 57.4 min, and 2.8 h, respectively (Figure 1).

Prepreg Manufacturing and Tensile Properties Characterization

Neat PA6 tensile specimens of ASTM D638 type IV were prepared by injecting the molten PA6 into a heat mold, which is portable and whose cooling rate can be easily controlled.

The prepreg was manufactured using the melt impregnation method with fiber bundles passing through the cross-head impregnation die designed by us. The width, thickness, and fiber volume fraction of the prepreg were fixed to be 7.00 ± 0.15 mm, 0.25 ± 0.03 mm, and 50.0 ± 2.0%, respectively.

The tensile tests were performed on a universal test machine (WDW-100, Changchun Kexin Co., Ltd.) according to ASTM D638 for neat PA6 and ASTM D3039 for CF/PA6 composites, respectively. The cross-head speed was 5 mm/min for PA6 and 1 mm/min for CF/PA6, and at least five specimens of each group were tested. The fracture surfaces of the failed prepregs were examined by Apolo 6010 scanning electron microscope (SEM).

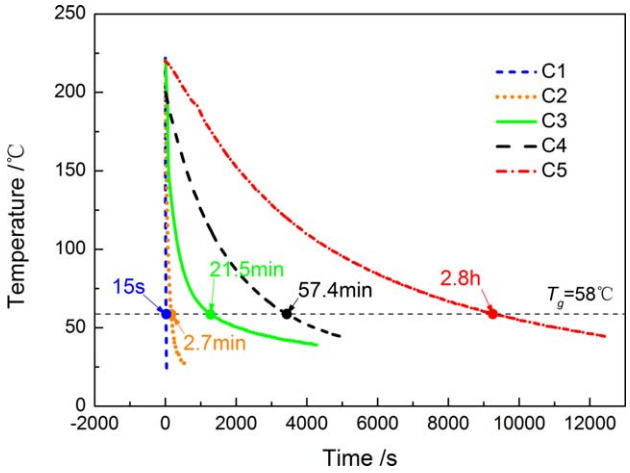

Figure 1. Five different cooling histories monitored by μ-thermocouple for preparing CF/PA6 specimens. [Color figure can be viewed in the online issue, which is available at wileyonlinelibrary.com.]

Polarizing Optical Microscopy

The POM specimens were prepared by placing a single carbon fiber between two thin PA6 films on a glass slide. After PA6 was heated to melt and kept for 3 min on a hot stage to eliminate the thermal history, a cover glass was placed on it. Then, the resin containing the single carbon fiber was pressed onto a 50–100 μm thick film and cooled. The crystal morphology was observed using a Leica DM4000M polarizing microscope.

Interfacial Nanomechanical Characterization

The CF/PA6 composite specimens for interfacial nanomechanical characterization were prepared by mounting the well impregnated and low fiber prepregs in epoxy. The cross-sections were then polished.

The interfacial nanomechanical behaviors of the CF/PA6 composites was measured on an *in situ* nanomechanical test system (Hysitron Inc., TI-900 TriboIndenter) under both SNI and DMI modes. The SNI was executed by penetrating a probe of 50 nm radius into a specific area with a maximum force of 1000 μN. The penetration depth was synchronously recorded with the applied force. The DMI was performed to obtain a modulus image of the selected area with the dimensions of 10 μm × 10 μm. A probe with a radius of 50 nm scanned the surface at a constant normal force of 2 μN with a superimposed dynamic force of 1 μN at 200 Hz. The distance between the two DMI neighboring indentation points was about 40 nm in both the *X* and *Y* directions.

RESULTS AND DISCUSSION

Effect of Cooling Rate on the Tensile Behaviors of PA6 and CF/PA6

The tensile results for the neat PA6 and CF/PA6 prepregs at different cooling rates are shown in Figure 2 and Table I. It was observed that the moduli of both the neat PA6 and CF/PA6 prepregs increased with a decrease in the cooling rate. It can be attributed to the high crystallinity obtained at low cooling rates. However, the strength showed a maximum value at C4 for neat PA6 and at C3 for CF/PA6 prepregs, respectively. This is because

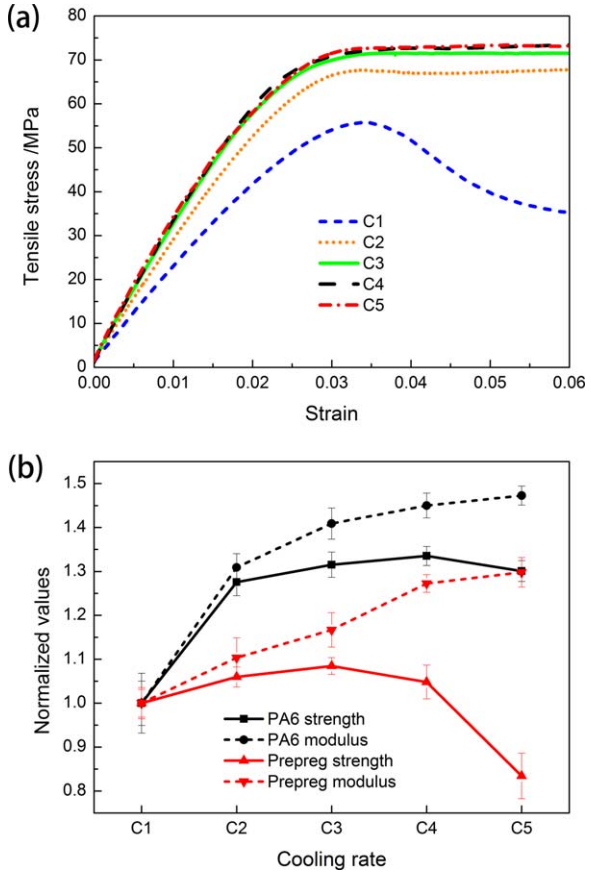

Figure 2. Tensile results for (a) neat PA6 stress–strain curves and (b) strengths and moduli of neat PA6 and CF/PA6 prepregs at different cooling rates. [Color figure can be viewed in the online issue, which is available at wileyonlinelibrary.com.]

high crystallinity can induce much defects and residual stress at crystal boundaries or inside the spherulites formed in the matrix, which can easily result in fracture failure at low cooling rates.[29] In the case of the CF/PA6 prepregs, the cooling rate for achieving the maximum strength was faster than that in the case of neat PA6. This may be attributed to the good crystallization inducing properties of carbon fibers.

The SEM images and sketch maps for the typical failure mechanism variations in the CF/PA6 composite tensile test affected by the cooling rate are shown in Figure 3. C1 shows the weak matrix indicated by the commonly yielded polymers, and poor interface adhesion suggested by the smooth fiber surfaces. With a decrease in the cooling rate, C3 showed good interfacial bonding and high tensile properties indicated by the large polymers sticking on the fiber surfaces and the destroyed matrices absorbing huge tensile failure energy. C5 showed relatively low tensile strength compared to C3, which is reflected by the less residual polymer on the fiber surface and a flat failure cross-section due to high crystallinity.

On the basis, of the results obtained from the aforementioned tests for the macroscopic mechanical properties, it can be concluded that cooling rate has a great effect on the mechanical properties of CF/PA6 composites. This is attributed to the

Table I. Parameters for Neat PA6 and CF/PA6 Composites with Different Cooling Rates

Parameter	Matrix strength	Matrix modulus	Prepreg strength	Prepreg modulus	Transcrystallinity thickness	Interphase thickness	Interphase modulus	Transcrystallinity modulus
Unit	σ_m (MPa)	E_m (GPa)	σ_p (MPa)	E_p (GPa)	h_{tc} (μm)	h_{ip} (nm)	E_{ip}/E_f	E_{tc}/E_f
T700	4900	230			—	—	1.000	1.000
C1	55.5 ± 2.8	2.20 ± 0.15	1784 ± 56	89.9 ± 3.2	3.3 ± 0.6[a]	389 ± 102[a]	0.232 ± 0.017	0.118 ± 0.005
C2	70.8 ± 2.2	2.88 ± 0.09	1891 ± 90	99.2 ± 4.5	10.9 ± 2.7	345 ± 115	0.250 ± 0.015	0.170 ± 0.006
C3	73.0 ± 2.1	3.10 ± 0.11	1935 ± 37	104.8 ± 4.1	15.4 ± 2.2	329 ± 89	0.282 ± 0.010	0.178 ± 0.004
C4	74.1 ± 1.6	3.19 ± 0.09	1870 ± 72	114.4 ± 2.3	19.3 ± 3.9	324 ± 108	0.286 ± 0.012	0.182 ± 0.003
C5	72.2 ± 1.7	3.24 ± 0.07	1489 ± 77	116.7 ± 3.9	21.8 ± 3.4	320 ± 98	0.295 ± 0.008	0.185 ± 0.004

[a] Standard errors of TC thickness and interphase thickness represent the thickness variation in one measured image, which can well describe the TC and interphase dimensions.

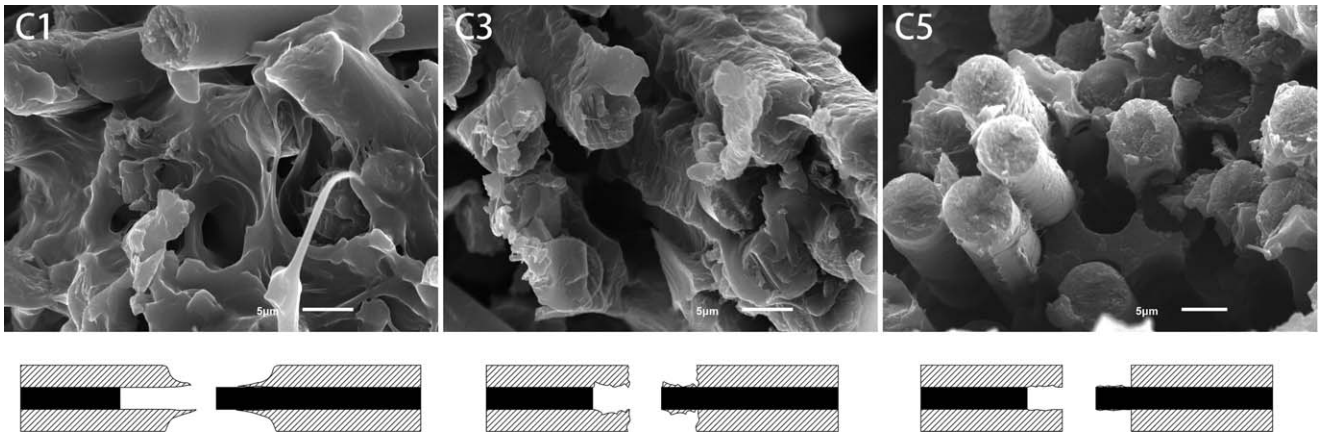

Figure 3. Sketch maps for the variation of CF/PA6 composite tensile failure mechanism affected by the cooling rate.

different crystallization behaviors at the fiber surface and in the matrix. Hence, the effect of cooling rate on the properties of regions near the fiber was examined from the microscopic point of view. The relationship between the micromechanical and the macromechanical properties were also elucidated.

Polarizing Optical Microscopy

Due to the intrinsic crystallization of semicrystalline thermoplastics, TC is universally reported at fiber surface, and the crystallization mechanism of TC is similar to that of spherulites in the bulk polymer.[29] However, the TC properties are considered to be different from those of the matrix materials outside the TC zone, since the transcrystalline zone is anisotropic because of molecular orientation.[32] This makes the PA6 matrix adjacent to the carbon fiber anisotropic.

To visually illustrate the anisotropic interface morphology and determine the TC thickness, first, POM was implemented and the results are shown in Figure 4. The transcrystallization was obvious in the CF/PA6 composites. Additionally, a decrease in the cooling rate resulted in the formation of larger spherulites and transcrystals in the matrix and on fiber surface, respectively. However, the nucleus density decreased for both. This is because the decreasing cooling rate results in a lower supercooling degree. However, polymers take longer time to crystallize and grow into larger crystals. The TC thickness was measured to be 3.3 ± 0.6, 10.9 ± 2.7, 15.4 ± 2.2, 19.3 ± 3.9, and 21.8 ± 3.4 μm for the specimens with five different cooling rates of C1, C2, C3, C4, and C5, respectively using an image manipulation software. Besides, the TC thickness showed a variation trend similar to that of the neat PA6 modulus, as shown in Figure 5.

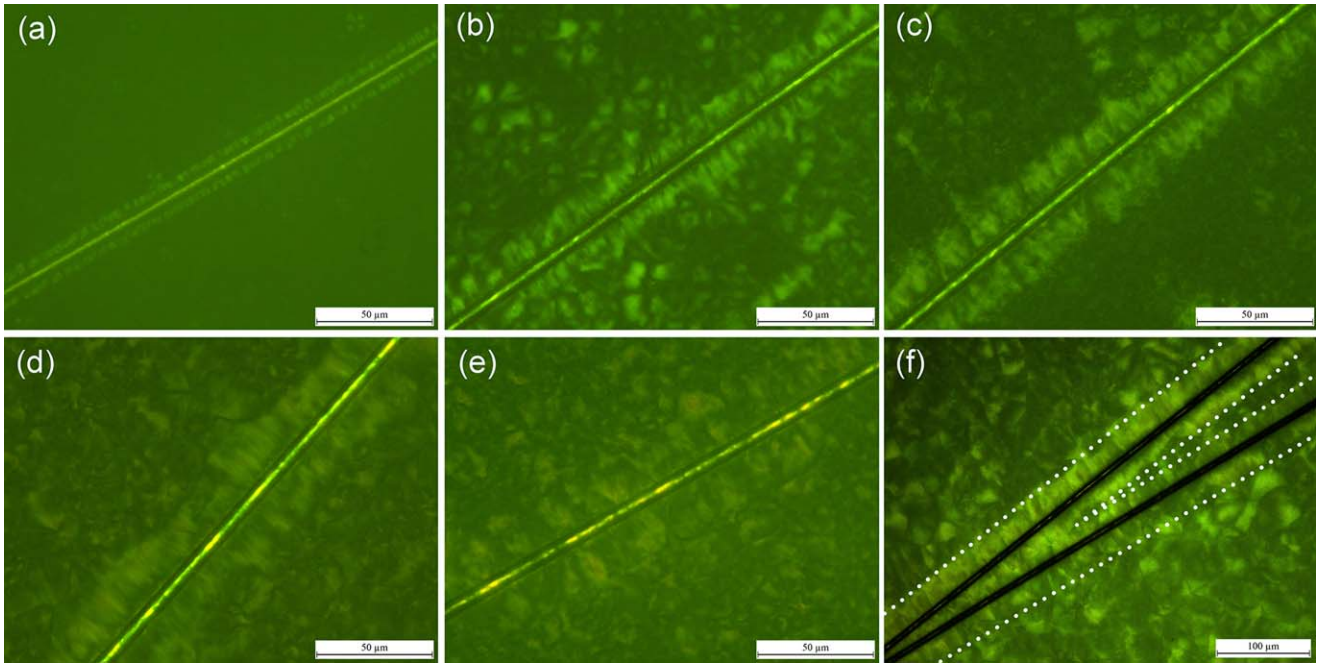

Figure 4. POM images of CF/PA6 single fiber composites at five different cooling rates of (a) C1, (b) C2, (c) C3, (d) C4, (e) C5, and (f) transcrystallization between two neighbor fibers. [Color figure can be viewed in the online issue, which is available at wileyonlinelibrary.com.]

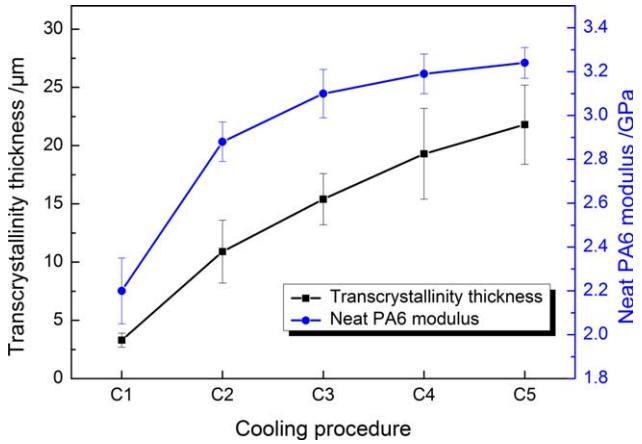

Figure 5. Variations in transcrystallinity thickness and neat PA6 modulus with cooling rate (the error bar of the TC thickness represents the thickness variation in one POM image). [Color figure can be viewed in the online issue, which is available at wileyonlinelibrary.com.]

This proves that the increase in the moduli of both PA6 and the composites was indeed caused by an increase in the crystallinity.

On the basis of the POM results, it can be speculated that there were at least four interfacial characteristic regions, that is, the carbon fiber region, interphase region, TC region and bulk matrix region outside the TC. This made the PA6 matrix modulus uneven.

Static Nanoindentation

To verify the above speculation, the SNI was implemented by investigating the indentation behaviors of different characteristic regions. In general, if the actual fraction of the fibers was greater than the critical volume fraction, there were no spherulites and only the TC was formed in the matrix as shown in Figure 4(f). As a result, the characteristic region of the bulk matrix outside the TC could not be tested. Therefore, the composites with quite low fiber volume fractions were employed here. The SNI results are shown in Figure 6. It can be seen that lower modulus and hardness were obtained for the regions gradually moving away from the carbon fiber, as indicated by the increased penetration depth and residual depth in Figure 6(b). Interestingly, the indentation response of the fiber center was also found to be different from that of the fiber periphery because of different oxidation degrees in the core and skin zones during the preparation.[30,33] Additionally, the bulk matrix outside the TC also showed three distinguished indentation responses for spherulites, amorphous PA6, and hybrid PA6 composed of imperfect spherulite and amorphous PA6, respectively. Finally, the seven characteristic regions [i.e., the fiber center, fiber periphery, interphase, TC, spherulite in the bulk matrix outside the TC, hybrid PA6 matrix outside the TC, and amorphous PA6 outside the TC, as schematically shown in Figure 6(a)] were clearly distinguished by their different indentation response behaviors as obtained from the SNI test. The results also demonstrated that the properties, such as the modulus and hardness of the transcrystalline region were very different from those of bulk matrix outside the TC because of high nucleus density at the fiber surface.

The amorphous PA6 modulus of 3.53 GPa approached the nominal moduli (see Table I). However, the fiber modulus was much smaller than the nominal modulus (230 GPa) for T700. This difference can be attributed to several reasons. First, although the important parameters of the instrument had been calibrated before measuring, the shape or radius of the topmost tip of the indenter might not be accurate enough because of the abrasion caused by repeated measurements. Second, the nanoscale penetration depth strongly influenced the calculated modulus because of the surface roughness and the discrepancy in the structure of the surface and bulk materials.[8,9,34] This was also verified by penetrating the topmost tip of the indenter into the carbon fiber to different depths, as shown in Figure 6(c). It was found that the hardness became constant only when the depth was greater than 30 nm, while the modulus was still steadily falling. Third, it is most likely that as a result of the different measuring mechanisms, the modulus value measured by the means of the nanoindentation method was different from the nominal static modulus value obtained by the tensile approach. It has been reported that for carbon fibers, the compression moduli are much lower than the tensile moduli.[35]

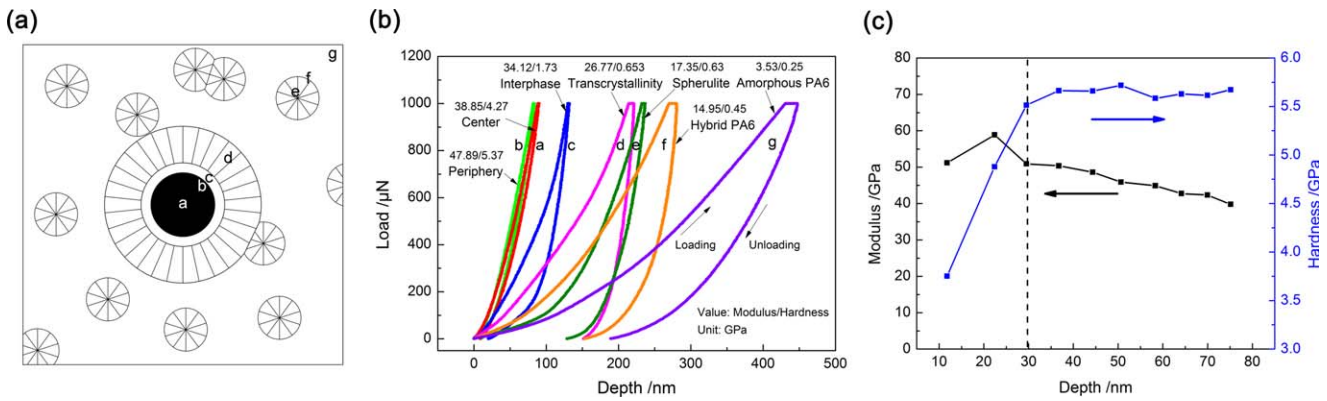

Figure 6. SNI test for (a) schematic diagram of seven interfacial characteristic regions (a: fiber center, b: fiber periphery, c: interphase, d: transcrystalline region, e: spherulite in matrix, f: hybrid matrix, g: amorphous matrix), (b) penetration response and typical modulus and hardness of the seven interfacial characteristic regions, and (c) the dependence of the modulus and hardness on the penetration depth in the SNI test. [Color figure can be viewed in the online issue, which is available at wileyonlinelibrary.com.]

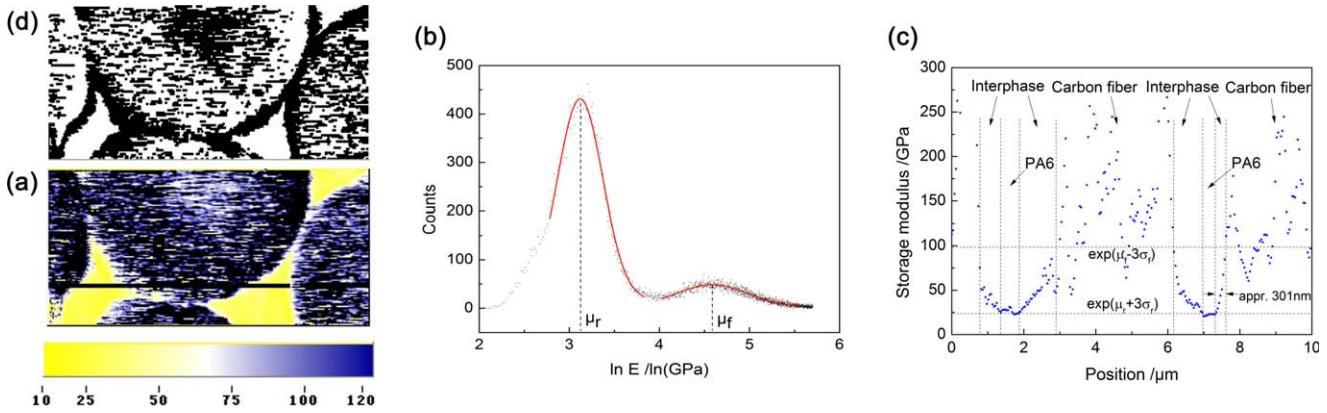

Figure 7. DMI result of (a) a storage modulus map in a selected characterization area of a the T700 CF/PA6 composite, (b) number statistics of the storage moduli in (a,c) the moduli for a line scan through the center of the fiber in (a,d) the extracted interphase in (a). [Color figure can be viewed in the online issue, which is available at wileyonlinelibrary.com.]

Although the measured moduli were obviously different from the nominal data, the values were stable, repeatable, and were consistent with the others.[8,30] Besides, the residual depth was the smallest. These are all the signature descriptions of carbon fibers.

Dynamic Mechanical Imaging

Thickness. Figure 7(a) shows the storage modulus map of the single T700 carbon fiber reinforced PA6 composite sample. The three phases of the matrix, fiber, and the intermediate interphase were clearly distinguished by yellow, blue, and white colors, respectively. The modulus of the matrix was much lower than that of the other two. By presenting the moduli in a line running across the right fiber center in Figure 7(a), the interphase displayed a modulus gradient between the two obvious storage modulus platforms for the matrix and the fiber, respectively. Additionally, the interphase was several hundred nanometers thick, as shown in Figure 7(c). The wide scatter for the carbon fiber moduli was due to nonuniform structure of the carbon fiber cross-section and the small indentation depth of several nanometers.

To further determine the interphase thickness of the CF/PA6 composite, the modulus counts of each DMI image were statistically analyzed, as illustrated in Figure 7(b). The moduli corresponding to the two fitting peaks were recognized as the matrix average modulus, μ_r, and carbon fiber average modulus, μ_f, respectively. Furthermore, the interphase was extracted according to a lower limit modulus of $\mu_r + 3\sigma_r$, and an upper limit modulus of $\mu_f - 3\sigma_f$,[8] where σ_r and σ_f denote the standard deviation of the natural logarithm of the moduli for the resin and fiber, respectively. The extracted CF/PA6 interphase shown in Figure 7(d) appears circular but uneven in thickness because of the surface topography of the T700 carbon fiber and nonuniformly distributed sizing on it. All the average interphase thicknesses, which were obtained from 60 to 80 random measurements on each interphase image, were in the range of 320–389 nm (Figure 8). They are much greater than that of the CF/epoxy (CF/EP) system.[8] This can be ascribed to the fact that the CF/PA6 interphase was formed by physical interaction rather than chemical bonding, and it was difficult to form narrow and dense interphase for the interdiffusion between PA6 and the epoxy sizing. The decreasing cooling rate resulted in thinner interphase because of the longer time for the interaction of PA6 with the carbon fibers. However, the thickness became stable at the C3 cooling rate.

Modulus. Although the average modulus standing for each interfacial characteristic region of a specimen could be obtained from the DMI results by a statistical estimation, it could not be directly used to compare the moduli of the specimens with different cooling rates. It is because of the influences of different surface roughness conditions and penetration depths among the specimens. In the DMI test, the theoretical depth of the DMI probe was less than 5 nm, which is quite a harsh requirement for the surface roughness of the polished specimen. Although the surface quality was controlled to reach the recommended roughness of 5–10 nm,[8] we could still not be sure that each specimen as well as the areas within the specimens had the same surface roughness condition. As a result, this notable difference was investigated even for a certain characteristic region with the same cooling rate. For example, the carbon fiber

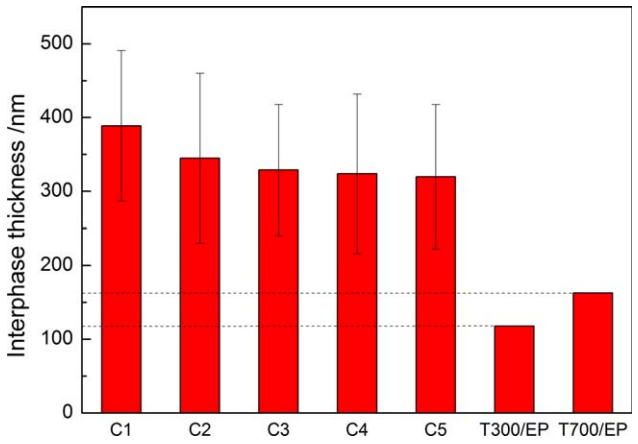

Figure 8. Interphase thickness for CF/PA6 composites with different cooling rates and CF/EP composites in Ref. 8. [Color figure can be viewed in the online issue, which is available at wileyonlinelibrary.com.]

Table II. Modulus Values for Each Interfacial Characteristic Region of Three C5 Cooled CF/PA6 Specimens (GPa)

	C5-1		C5-2		C5-3		
Interfacial characteristic region	DMI modulus	Normalized modulus	DMI modulus	Normalized modulus	DMI modulus	Normalized modulus	Average normalized modulus
Fiber	106.75	1.000	100.17	1.000	115.30	1.000	1.000
Interphase	31.26	0.293	29.35	0.293	34.57	0.300	0.295
0.5–1 μm	20.56	0.193	18.43	0.184	21.10	0.183	0.186
1–2 μm	19.88	0.186	18.03	0.180	21.35	0.185	0.184
2–3 μm	20.32	0.190	18.63	0.186	20.89	0.181	0.186
3–4 μm	19.76	0.185	18.13	0.181	21.15	0.183	0.183

moduli of the C5 specimens were found to be 106.75, 100.17, and 115.30 GPa (Table II).

To successfully investigate the influence of the cooling rate on the interphase modulus and detect the modulus variation trend from fiber via TC to matrix, the method shown in Figure 9(a) was employed. The average moduli of carbon fiber, interphase, and regions 0.5–1, 1–2, 2–3, and 3–4 μm away from the fiber surface of each DMI image were calculated. The moduli so obtained were then normalized with the corresponding carbon fiber moduli of the same DMI image, since the moduli of the carbon fibers in all the specimens could be considered as a constant because of negligible influence by the thermal treatment and matrix crystallization. As a result, the normalized values quite approached each other for a certain characteristic region with the same cooling rate. The average values of the normalized results for each characteristic region are shown in Table I and Figure 9(b). It is worth noting that the DMI image containing the isolated fiber was preferentially used here because the entire interphase and more matrix information could be well obtained when the neighboring fibers were absent.

It can be seen from Figure 9(b) that notable modulus gaps were present between the fiber, interphase, and matrix. This observation was consistent with the SNI results. The moduli of the interphase and TC were in the grade of 0.23–0.30 times and 0.12–0.19 times that of the fiber, respectively.

The moduli of the interphase and TC increased with the decreasing cooling rate. Additionally, the interphase modulus of the fast quenched C1 sample was still the lowest though the TC looked quite dense and had a high nucleation density, as observed from the POM analysis. The TC moduli showed stable values for the C2, C3, C4, and C5 specimens, while a weak drop was observed in the region of 3–4 μm for the C1 specimens. This is consistent with the measured TC thickness of 3.3 μm listed in Table I, and also implies that the CF/PA6 matrix was not isotropic. In practical applications of the composites with a large fiber volume fraction, the distance between the two neighboring fibers is usually less than 7 μm, and all the fibers are linked by transcrystals, as shown in Figure 4(f). So, a drop in the TC modulus might not occur in practical fast cooling composites.

According to Syed Asif,[30] the moduli calculated from the scanned images are in excellent agreement with the indentation measurements for the storage modulus. In this study, the obtained TC moduli were indeed close to those obtained by the SNI mode. However, the lowest modulus of the C1 cooled PA6 in the 3–4 μm region was still much higher than that of the amorphous PA6 (3.53 GPa) obtained by the SNI from the bulk

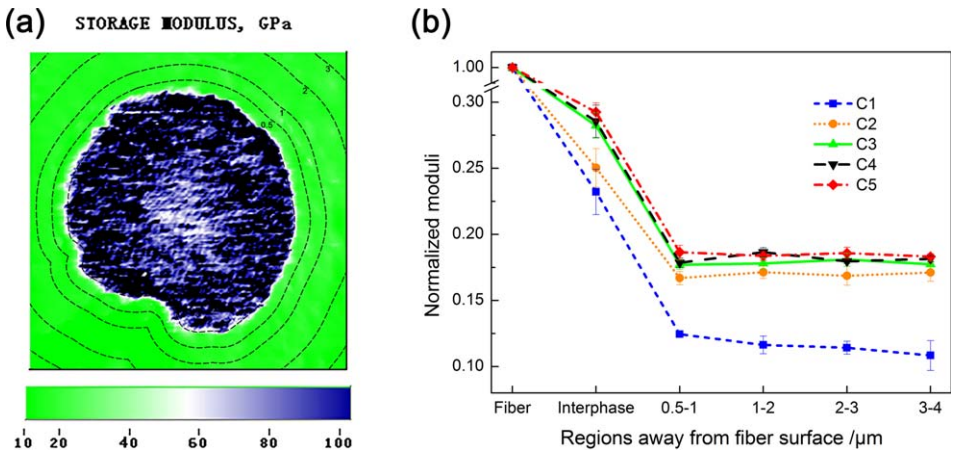

Figure 9. DMI test for (a) statistics regions in the CF/PA6 composite and the (b) modulus of fiber, interphase, and different PA6 regions away from the carbon fiber surface for CF/PA6 composites with different cooling rates. [Color figure can be viewed in the online issue, which is available at wileyonlinelibrary.com.]

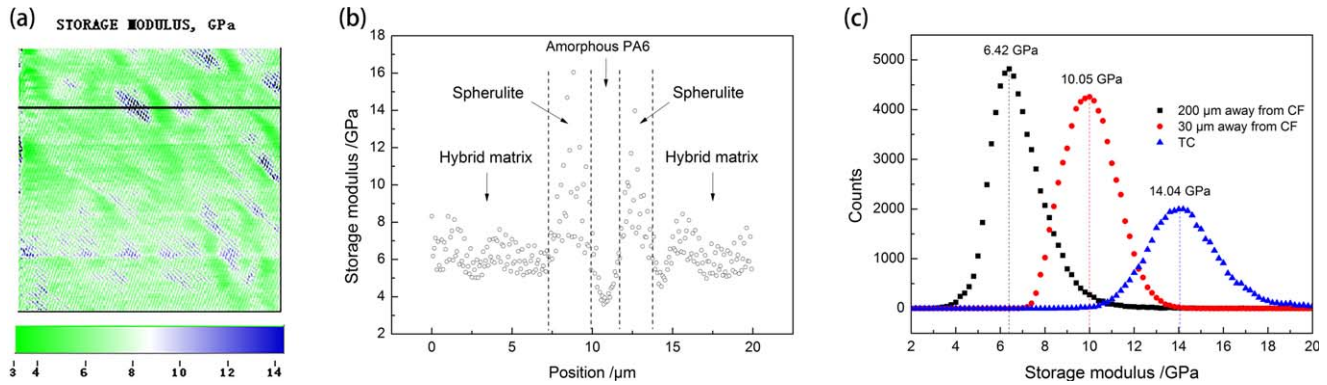

Figure 10. DMI results for a C1 specimen of (a,b) matrix modulus distribution for a 20 μm × 20 μm region 200 μm away from transcrystallinity, and (c) matrix modulus variation with distance away from the carbon fiber. [Color figure can be viewed in the online issue, which is available at wileyonlinelibrary.com.]

matrix far away from the fiber. This is because this region was located at the transition area from TC to the bulk matrix and the crystalline phase was still the main composition. Thus, the modulus values of the two 20 μm × 20 μm regions more than 3.3 μm away from the fiber surface on one C1 specimen were separately investigated, as shown in Figure 10. As can be seen from Figure 10(a,b), the matrix was composed of three alternate regions of low modulus of 3.60 GPa (0.03 times that of the carbon fiber) for the amorphous PA6, high modulus of 16.05 GPa for the spherulites, and the intermediate phase of 6.42 GPa resulting by the hybridization of the other two at nanoscale. In addition, the average matrix modulus was increased and gradually approached to the TC modulus with the regions close to the carbon fiber [see Figure 10(c)]. This implies that in the bulk matrix outside the TC, the crystalline component increased close to the carbon fiber, which proves its anisotropy. By far, all the DMI results were in good agreement with the SNI results.

The moduli of the TC were higher than those of the bulk matrix containing the spherulites and amorphous PA6 because the molecular conformation in the transcrystalline region was composed of highly aligned crystalline zig-zag polymer molecules induced by the high nuclear density at the fiber surface. It is reported that the modulus parallel to the chain direction is much (maximum can up to 100 times[23]) greater than that perpendicular to the chain axis.[21–23,26,36,37] Then a hybrid contribution resulted in the much higher average modulus than that of the bulk matrix outside the TC, where the strong mechanical anisotropy of the crystalline component was averaged by randomly distributed spherulitic texture and amorphous PA6.

From Figure 9(b), it can also be seen that the moduli of the TC and interphase became steady for C2 and C3. This is consistent with the macroscopic mechanical results, which showed that the composite strength began stabilizing from C2 and showed a maximum value at C3. It also suggests that a short time of about 2.7 min was enough to form a stable TC in the CF/PA6 composite; however, a little more time was still needed to reach the optimum tensile behavior.

CONCLUSIONS

The macroscopic mechanical tests of the neat PA6 and CF/PA6 prepregs showed that the cooling rate significantly affects the mechanical properties of the CF/PA6 composites. The moduli of both the neat PA6 and CF/PA6 prepregs increased with the decreasing cooling rate, while the strength showed a maximum value at C4 for neat PA6 and at C3 for the CF/PA6 prepregs, respectively. Transcrystallization was clearly observed in the CF/PA6 composites. The TC thickness was measured to be 3.3 ± 0.6, 10.9 ± 2.7, 15.4 ± 2.2, 19.3 ± 3.9, and 21.8 ± 3.4 μm for the C1–C5 specimens, respectively. Seven characteristic regions were clearly distinguished from different indentation response behaviors from the SNI test. The moduli of the interphase, TC and amorphous PA6 were successfully calculated to be 0.23–0.30, 0.12–0.19, and 0.03 times that of the carbon fiber compression modulus, respectively using the DMI technology. The interphase thickness of the CF/PA6 composites was in the range of 320–389 nm and decreased with a decrease in the cooling rate. On the contrary, the thickness of the TC and the modulus of interphase and TC showed significant increases with a decrease in the cooling rate. The results of the nanomechanical tests (DMI and SNI) showed good agreements with each other and with the macromechanical tests. The experimental results were expected to provide some useful parameters for simulation for establishing an anisotropic model for further studies. They were also expected to provide some theoretical guidance for the manufacturing of CF/PA6 composite with desired properties by controlling the cooling rate and realizing their practical applications.

REFERENCES

1. Colucci, G.; Ostrovskaya, O.; Frache, A.; Martorana, B.; Badini, C. *J. Appl. Polym. Sci.* **2015**, *132*, DOI: 10.1002/app.42275.
2. Ranganathan, N.; Oksman, K.; Nayak, S. K.; Sain, M. *J. Appl. Polym. Sci.* **2015**, *132*, DOI: 10.1002/app.41301.
3. Sönmez, M.; Georgescu, M.; Vâlsan, M.; Radulescu, M.; Ficai, D.; Voicu, G.; Ficai, A.; Alexandrescu, L. *J. Appl. Polym. Sci.* **2015**, *132*, DOI: 10.1002/app.42163.
4. Markarian, J. *Plast. Eng.* **2011**, *9*, 22.
5. Wu, Q.; Li, M.; Gu, Y. Z.; Wang, S. K.; Wang, X. X.; Zhang, Z. G. *J. Appl. Polym. Sci.* **2015**, *132*, DOI: 10.1002/app.41917.

6. Yu, X.; Gu, B.; Zhang, B. *J. Appl. Polym. Sci.* **2015**, *132*, DOI: 10.1002/app.42774.
7. Qi, G. C.; Du, S. Y.; Zhang, B. M.; Tang, Z. W.; Yu, Y. L. *Compos. Sci. Technol.* **2014**, *105*, 1.
8. Gu, Y. Z.; Li, M.; Wang, J.; Zhang, Z. G. *Carbon* **2010**, *48*, 3229.
9. Gao, S. L.; Mäder, E. *Compos. Part A: Appl. Sci. Manuf.* **2002**, *33*, 559.
10. Bogetti, T. A.; Wang, T.; VanLandingham, M. R.; Gillespie, J. W. *Compos. Part A: Appl. Sci. Manuf.* **1999**, *30*, 85.
11. Zhang, B.; Gu, B. Q. *Appl. Mech. Mater.* **2011**, *55*, 303.
12. Wang, W.; Sadeghipour, K.; Baran, G. *Compos. Part A: Appl. Sci. Manuf.* **2008**, *39*, 956.
13. Daoust, J.; Vu-Khanh, T.; Ahlstrom, C.; Gerard, J. F. *Compos. Sci. Technol.* **1993**, *48*, 143.
14. Ho, H.; Drzal, L. T. *Compos. Eng.* **1995**, *5*, 1231.
15. Ho, H.; Drzal, L. T. *Compos. Eng.* **1995**, *5*, 1245.
16. Kim, J. K.; Mai, Y. W. Engineered Interfaces in Fiber Reinforced Composites; Elsevier, **1998**; Chapter 7.3.1, p 300.
17. Yu, X.; Gu, B.; Zhang, B. *J. Appl. Polym. Sci.* **2015**, *132*, 41638.
18. Gao, Y.; Wu, Y.; Liang, M. Q.; Fu, Q. *J. Appl. Polym. Sci.* **2015**, *132*, DOI: 10.1002/app.42119.
19. Nielsen, A. S.; Pyrz, R. *J. Mater. Sci.* **2003**, *38*, 597.
20. Gao, S. L.; Kim, J. K. *Compos. Part A: Appl. Sci. Manuf.* **2000**, *31*, 517.
21. Sheng, N.; Boyce, M. C.; Parks, D. M.; Rutledge, G. C.; Abes, J. I.; Cohen, R. E. *Polymer* **2004**, *45*, 487.
22. Vendramini, J.; Mele, P.; Merle, G.; Alberola, N. D. *J. Appl. Polym. Sci.* **2000**, *77*, 2513.
23. Amitay-Sadovsky, E.; Cohen, S. R.; Wagner, H. D. *Appl. Phys. Lett.* **1999**, *74*, 2966.
24. Amitay-Sadovsky, E.; Wagner, H. D. *J. Polym. Sci. Part B: Polym. Phys.* **1999**, *37*, 523.
25. Amitay-Sadovsky, E.; Wagner, H. D. *Polymer* **1998**, *39*, 2387.
26. Tzika, P. A.; Boyce, M. C.; Parks, D. M. *J. Mech. Phys. Solids* **2000**, *48*, 1893.
27. Muratoğlu, O. K.; Argon, A. S.; Cohen, R. E. *Polymer* **1995**, *36*, 2143.
28. Gao, S. L.; Kim, J. K. *J. Appl. Polym. Sci.* **2002**, *84*, 1155.
29. Li, H. F.; Zhang, Y. F.; Wang, Y.; Zhang, B. M. *Polym. Compos.* **2016**, DOI: 10.1002/pc.23907.
30. Syed Asif, S. A.; Wahl, K. J.; Colton, R. J.; Warren, O. L. *J. Appl. Phys.* **2001**, *90*, 1192.
31. Ţălu, Ş. Micro and Nanoscale Characterization of Three Dimensional Surfaces. Basics and Applications; Napoca Star Publishing House: Cluj-Napoca, Romania, **2015**.
32. Yu, Z.; Ait-Kadi, A.; Brisson, J. *Polym. Eng. Sci.* **1991**, *31*, 1228.
33. Wang, Y.; Hahn, T. H. *Compos. Sci. Technol.* **2007**, *67*, 92.
34. Clifford, C. A.; Seah, M. P. *Appl. Surf. Sci.* **2005**, *252*, 1915.
35. Oya, N.; Johnson, D. J. *Carbon* **2001**, *39*, 635.
36. Van Dommelen, J. A. W.; Brekelmans, W. A. M.; Baaijens, F. P. T. *Mech. Mater.* **2003**, *35*, 845.
37. Amitay-Sadovsky, E.; Zheng, S.; Smith, J.; Wagner, H. D. *Acta Polym.* **1998**, *49*, 588.